

PDE-BASED INTERPOLATION METHOD FOR OPTICALLY VISUALIZED SOUND FIELD

Kohei Yatabe and Yasuhiro Oikawa

Department of Intermedia Art and Science, Waseda University, Tokyo, Japan

ABSTRACT

An effective way to understand the behavior of a sound field is to visualize it. An optical measurement method is a suitable option for this as it enables contactless non-destructive measurement. After measuring a sound field, interpolation of the data is necessary for a smooth visualization. However, conventional interpolation methods cannot provide a physically meaningful result especially when the condition of the measurement causes moiré effect. In this paper, a special interpolation method for an optically visualized sound field based on the Kirchhoff-Helmholtz integral equation is proposed.

Index Terms— Sound field visualization, partial differential equation (PDE), laser Doppler vibrometer (LDV), Schlieren imaging.

1. INTRODUCTION

Understanding the behavior of a sound field is one of the most important tasks for many acousticians. Microphones are usually used for such observation; however, the presence of measuring instruments inside the sound field prevents accurate measurement because a sound field depends on the spatial setting of the field. As an alternative, optical observation for audible sound field have been developed recently including Schlieren imaging [1, 2] and Optophone [3, 4]. Our research group is developing the laser measurement method using a laser Doppler vibrometer (LDV) [5, 6]. These methods enable a contactless non-destructive measurement of sound field by detecting fluctuations on optical quantity caused by the sound field such as diffraction and Doppler shift. Common characteristic among these optical methods is that the measured data represent physical quantity of a sound field integrated along a beam of measuring light. Although some applications may require three-dimensional information which leads to collaboration with computed tomography (CT) [5, 7, 8, 9, 10], two-dimensional visualization of the sound field is still a highly effective tool for its qualitative evaluation. This paper focuses on a visualized two-dimensional sound field projected by the optical methods.

When a measured sound field is displayed on a screen, post-processing of the measured data, typified by interpolation, is necessary since it is difficult to measure thousands or even millions of points for smooth appearance depicted on a several kilo- or mega-pixel display. Conventionally, polynomial interpolation, an extremely popular method in image processing which fits a polynomial function to data, is applied to optically visualized sound fields for a smoother presentation. However, polynomial interpolation cannot always provide a good approximation of an actual sound field especially when the condition causes a moiré effect.

In this paper, a special interpolation method for an optically visualized sound field based on the Kirchhoff-Helmholtz integral equation is proposed. Experiments confirm its effectiveness and robustness against noise.

2. OPTICAL PROJECTION OF SOUND FIELD

When a sound field is projected by a light beam, physical quantity of the sound field, which in most cases is sound pressure variation, is integrated along the beam [11]. Let us consider a general model of optical measurement of a sound field governed by the homogeneous Helmholtz equation as in Fig. 1. There are rigid parallel planes at $z = 0$ and $z = d$ which reflect sounds completely. (The actual meaning of these planes varies depending on which measurement method is applied). Once a light beam is emitted from the plane at $z = 0$ perpendicularly, the sound field is integrated through $z = [0, d]$ as

$$\int_0^d (\nabla^2 + k^2)p(\mathbf{r}) dz = 0 \quad (1)$$

where p is sound pressure, k is the wave number, $\mathbf{r} \in \mathbb{R}^3$ is a position and $\nabla^2 = \partial^2/\partial x^2 + \partial^2/\partial y^2 + \partial^2/\partial z^2$ denotes the three-dimensional Laplacian operator. Using the Leibniz integral rule,

$$\left(\frac{\partial^2}{\partial x^2} + \frac{\partial^2}{\partial y^2} + k^2 \right) \int_0^d p(\mathbf{r}) dz = -\alpha \int_0^d \frac{\partial v_z(\mathbf{r})}{\partial z} dz, \quad (2)$$

and this can be rearranged as

$$(\nabla_{2D}^2 + k^2) \int_0^d p(\mathbf{r}) dz = -\alpha [v_z(\mathbf{r})]_{z=0}^{z=d} \quad (3)$$

where $v_z(\mathbf{r}) = 1/i\omega\rho_0 \cdot \partial p(\mathbf{r})/\partial z$ is the z -way (which is also the normal direction to the planes) particle velocity, $\alpha = i\omega\rho_0$ and $\nabla_{2D}^2 = \partial^2/\partial x^2 + \partial^2/\partial y^2$. As we assumed complete reflection on the boundaries, the right-hand side of Eq. (3) becomes zero, and we obtain

$$(\nabla_{2D}^2 + k^2) p_{proj} = 0 \quad (4)$$

with $p_{proj} = \int_0^d p(\mathbf{r}) dz$. This result indicates that a projected sound field, originally governed by the three-dimensional Helmholtz equation, is dominated by the two-dimensional Helmholtz equation. Therefore, it is reasonable to apply the two-dimensional Kirchhoff-Helmholtz equation to an optically projected sound field. In the rest of this paper, p denotes the projected sound pressure p_{proj} and $\mathbf{r} \in \mathbb{R}^2$ denotes a position in the interior of a two-dimensional region Ω .

3. INTERPOLATION METHOD FOR OPTICALLY PROJECTED SOUND FIELD

The Kirchhoff-Helmholtz integral equation

$$p(\mathbf{r}) = \int_{\partial\Omega} \left[G(\mathbf{r}, \mathbf{r}_b) \frac{\partial p(\mathbf{r}_b)}{\partial n} - \frac{\partial G(\mathbf{r}, \mathbf{r}_b)}{\partial n} p(\mathbf{r}_b) \right] d\mathbf{r}_b \quad (5)$$

is the boundary integral form of the Helmholtz equation where $\mathbf{r} \in \Omega$, $\mathbf{r}_b \in \partial\Omega$, G is the fundamental solution of the Helmholtz equation and $\partial/\partial n$ denotes the outward-directed normal derivative at the boundary. This equation implies that the sound pressure at any points

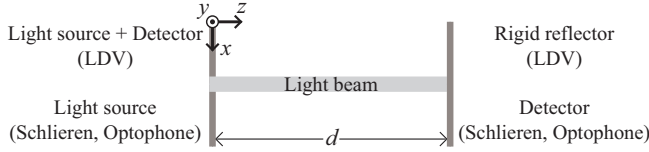


Fig. 1. Geometry of a general model of optical measurement of a sound field considered in Section 2.

in the interior of a region Ω can be calculated from the boundary condition since the fundamental solution G and its normal derivative are known from positions \mathbf{r} and \mathbf{r}_b as

$$G(\mathbf{r}, \mathbf{r}_b) = \frac{j}{4} H_0^{(1)}(k|\mathbf{r} - \mathbf{r}_b|) \quad (6)$$

$$\frac{\partial G(\mathbf{r}, \mathbf{r}_b)}{\partial n} = \frac{jk}{4} H_1^{(1)}(k|\mathbf{r} - \mathbf{r}_b|) \frac{(\mathbf{r} - \mathbf{r}_b) \cdot \mathbf{n}}{|\mathbf{r} - \mathbf{r}_b|} \quad (7)$$

in the two-dimensional case where \mathbf{n} is a unit normal vector at \mathbf{r}_b and $H_0^{(1)}$ denotes the Hankel function of the first kind of order zero. Therefore, using the Kirchhoff-Helmholtz integral equation, an interpolation problem of an optically projected sound field is reduced to the estimation problem of the boundary condition of an arbitrarily selected boundary surrounding the measured region.

With appropriate discretization, as in boundary element method, Eq. (5) can be expressed as a simultaneous linear equation

$$\mathbf{p} = \mathbf{G}\mathbf{p}_b \quad (8)$$

where \mathbf{G} is a matrix of G and $\partial G/\partial n$, \mathbf{p} is a vector containing interior sound pressure $p(\mathbf{r})$ and \mathbf{p}_b is the boundary condition to be estimated. This problem, however, cannot be solved simply because the condition number of \mathbf{G} exceeds 10^{15} . In order to solve this ill-posed problem, partial differential equation (PDE), the Helmholtz equation in this case, is utilized as an equality constraint on a least squares formulation. As a result, the problem to be solved becomes

$$\min_{\mathbf{p}_b} \|\mathbf{G}\mathbf{p}_b - \mathbf{p}\|^2 \quad \text{s.t.} \quad (\nabla^2 + k^2)p = 0 \quad (9)$$

where $\nabla^2 = \partial^2/\partial x^2 + \partial^2/\partial y^2$ and $\|\cdot\|$ denotes Euclidean norm.

3.1. Discretization of Kirchhoff-Helmholtz integral equation

One easy way to discretize Eq. (5) is combining

$$p(\mathbf{r}_i) = \mathbf{g}_i^T \mathbf{p}_b \quad (10)$$

into a matrix equation Eq. (8) where

$$\mathbf{p} = [p(\mathbf{r}_1) \ p(\mathbf{r}_2) \ \cdots \ p(\mathbf{r}_N)]^T,$$

$$\mathbf{G} = [\mathbf{g}_1 \ \mathbf{g}_2 \ \cdots \ \mathbf{g}_N]^T d,$$

$$\mathbf{g}_i = [G(\mathbf{r}_i, \mathbf{r}_{b_1}) \ \cdots \ G(\mathbf{r}_i, \mathbf{r}_{b_M}) - G'(\mathbf{r}_i, \mathbf{r}_{b_1}) \ \cdots - G'(\mathbf{r}_i, \mathbf{r}_{b_M})]^T,$$

$$\mathbf{p}_b = [p'(\mathbf{r}_{b_1}) \ p'(\mathbf{r}_{b_2}) \ \cdots \ p'(\mathbf{r}_{b_M}) \ p(\mathbf{r}_{b_1}) \ p(\mathbf{r}_{b_2}) \ \cdots \ p(\mathbf{r}_{b_M})]^T, \quad (11)$$

f' denotes $\partial f/\partial n$, $N \in \mathbb{N}\setminus\{0\}$ is the number of the measured points and $M \in \mathbb{N}\setminus\{0\}$ is the number of the arbitrarily selected points on a boundary for the discretization. However, this formulation cannot handle the Laplacian in Eq. (9) since it considers the boundary condition with points only at the boundary; values of discretization points only at the boundary cannot provide its gradient and divergence without knowing the underlying formula.

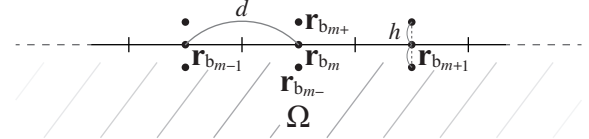


Fig. 2. Discrete points of the boundary condition $\mathbf{p}_{b\pm}$ in Section 3.2.

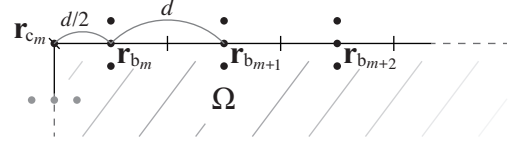


Fig. 3. Arrangement of discrete points around a corner in Eq. (14).

In order to approximate second-order derivatives from sampled values, at least three points are required in the direction of the derivative. Thus, points near the boundary \mathbf{r}_{b_+} and \mathbf{r}_{b_-} , which are located outside and inside the region in normal-direction respectively, are incorporated into the boundary condition \mathbf{p}_b . Figure 2 shows an example of the points at the boundary discretized with the midpoint rule and its neighborhoods. In this paper, a square-shaped boundary is chosen for a simpler notation of finite difference approximation of its tangent and normal derivatives.

3.2. Matrix formulation with finite difference approximation

Finite difference approximation of the homogeneous Helmholtz equation $(\nabla^2 + k^2)p = 0$ can be written as

$$\left[\frac{1}{h^2} \mathbf{I} \quad \left(\frac{-2}{h^2} \mathbf{I} + \mathbf{B} + k^2 \mathbf{I} \right) \quad \frac{1}{h^2} \mathbf{I} \right] \mathbf{p}_{b\pm} =: \mathbf{H} \mathbf{p}_{b\pm} = \mathbf{0} \quad (12)$$

where $h = \|\mathbf{r}_{b_{m+}} - \mathbf{r}_{b_m}\| = \|\mathbf{r}_{b_m} - \mathbf{r}_{b_{m-}}\|$, \mathbf{I} is the M -dimensional identity matrix, $\mathbf{p}_{b\pm}$ is a vector of sound pressure at \mathbf{r}_{b_+} , \mathbf{r}_b and \mathbf{r}_{b_-}

$$\mathbf{p}_{b\pm} = [p(\mathbf{r}_{b_{1+}}) \ \cdots \ p(\mathbf{r}_{b_{M+}}) \ p(\mathbf{r}_{b_1}) \ \cdots \ p(\mathbf{r}_{b_M}) \ p(\mathbf{r}_{b_{1-}}) \ \cdots \ p(\mathbf{r}_{b_{M-}})]^T,$$

and \mathbf{B} is the band matrix approximating second-order derivatives as

$$p^{(2)}(\mathbf{r}_{b_m}) = \frac{p(\mathbf{r}_{b_{m+1}}) - 2p(\mathbf{r}_{b_m}) + p(\mathbf{r}_{b_{m-1}})}{d^2} \quad (13)$$

where $d = \|\mathbf{r}_{b_{m+1}} - \mathbf{r}_{b_m}\| = \|\mathbf{r}_{b_m} - \mathbf{r}_{b_{m-1}}\|$ and $f^{(l)}$ denotes l -th order tangent derivatives. This band matrix is modified in order to handle corners of the box-shaped boundary properly by adding corner points $p(\mathbf{r}_c)$ which are only used for the constraint, not for the integration in Eq. (5), and using four-points difference

$$p^{(2)}(\mathbf{r}_{b_m}) = \frac{16p(\mathbf{r}_{c_m}) - 25p(\mathbf{r}_{b_m}) + 10p(\mathbf{r}_{b_{m+1}}) - p(\mathbf{r}_{b_{m+2}})}{5d^2} \quad (14)$$

where $\|\mathbf{r}_{b_m} - \mathbf{r}_{c_m}\| = d/2$ as in Fig. 3. The error term of this four points formula is $\frac{1}{24}d^2 p^{(4)}(\mathbf{r}_{b_m}) + O(d^3)$ which is the same order of the three points formula in Eq. (13): $\frac{1}{12}d^2 p^{(4)}(\mathbf{r}_{b_m}) + O(d^3)$.

Similarly, the normal derivative of sound pressure at the boundary $p'(\mathbf{r}_{b_m})$ in Eq. (11) can be approximated by finite difference

$$p'(\mathbf{r}_{b_m}) = \frac{p(\mathbf{r}_{b_{m+}}) - p(\mathbf{r}_{b_{m-}})}{2h}$$

which describes the relation between \mathbf{p}_b and $\mathbf{p}_{b\pm}$ as

$$\mathbf{p}_b = \begin{bmatrix} \frac{1}{2h} \mathbf{I} & \mathbf{0} \\ \mathbf{0} & \mathbf{I} \end{bmatrix} \mathbf{p}_{b\pm} =: \mathbf{D} \mathbf{p}_{b\pm}. \quad (15)$$

Therefore, including everything above, Eq. (9) finally becomes

$$\min_{\mathbf{p}_{b\pm}} \|\mathbf{G}\mathbf{D}\mathbf{p}_{b\pm} - \mathbf{p}\|^2 \quad \text{s.t.} \quad \mathbf{H}\mathbf{p}_{b\pm} = \mathbf{0}. \quad (16)$$

Although this kind of equality constrained quadratic programming problem can be solved directly, a direct approach is not suitable for Eq. (16) because the equality constraint equation is not exact but approximated which leads to instability of the solution. Hence, the constraint is integrated as a penalty term with Tikhonov regularizer

$$\min_{\mathbf{p}_{b\pm}} \|\mathbf{G}\mathbf{D}\mathbf{p}_{b\pm} - \mathbf{p}\|^2 + \alpha \|\mathbf{H}\mathbf{p}_{b\pm}\|^2 + \beta \|\mathbf{p}_{b\pm}\|^2 \quad (17)$$

where α and β are regularization parameters. The procedure of the proposed method is as follows:

1. Import measured data \mathbf{p} and calculate \mathbf{G} as in Eq. (11) from Eq. (6) and Eq. (7).
2. Create \mathbf{H} and \mathbf{D} illustrated in Eq. (12) and Eq. (15).
3. Solve Eq. (17) to estimate the boundary condition $\mathbf{p}_{b\pm}$.
4. Calculate any points inside the region from the estimated boundary condition using Eq. (5).

4. EXPERIMENTS

4.1. Numerical simulation

A numerical simulation was conducted to confirm effectiveness of the proposed method. The simulation condition is listed in Table 1. A projected sound field was sampled by 16×16 sampling points, and a box-shaped boundary was set around the sampling points as in Fig. 4. A point sound source was located at the lower left, and the sound field was reconstructed by interpolating the sampled points.

Figure 5 shows an example of a reconstructed sound field compared with ordinary polynomial interpolation methods: bilinear and third-order spline interpolation. Gaussian noise was added to the sound field generated by a 1500 Hz point sound source, and the noisy mixture was sampled as test data. Even though the sampling interval is shorter than the Nyquist interval, a moiré effect was observed on the results of polynomial interpolation methods, illustrated in Fig. 5(d) and 5(e). On the other hand, it can be confirmed that the proposed method clearly reconstructed the original field.

For the quantitative assessment, signal-to-noise ratio (SNR) of interpolated sound fields,

$$\text{SNR}_{\text{result}} = 10 \log_{10} \frac{\sum_{x,y} |p|^2}{\sum_{x,y} |p - \hat{p}|^2} \quad (18)$$

where p is the sound pressure of the original sound field and \hat{p} denotes the interpolated sound field, were calculated for several sampled fields with additional noise whose SNR,

$$\text{SNR}_{\text{sample}} = 10 \log_{10} \frac{\sum_{x,y} |p|^2}{\sum_{x,y} |w|^2} \quad (19)$$

where w denotes noise, set up arbitrarily by adjusting the level of Gaussian noise. Figure 6 shows SNR of the interpolated sound fields versus SNR of the sampled fields. $\text{SNR}_{\text{sample}}$ was calculated from $16 \times 16 = 256$ sampling points whereas $\text{SNR}_{\text{result}}$ was calculated from $301 \times 301 = 90601$ interpolated points. The peak signal-to-noise ratio, $\text{PSNR} = 10 \log_{10} \{ 90601 p_{\text{max}}^2 / \sum_{x,y} |p - \hat{p}|^2 \}$, was also illustrated in the same figure where p_{max} denotes the maximum possible value of the sound pressure inside the sampled region after normalization. For all of the data, the regularization parameters in Eq. (17) were fixed to $\alpha = 1$ and $\beta = 0.1$.

Table 1. Simulation condition.

Sampling points	$16 \times 16 (= 256)$ points
Sound source position	$(-1, -1)$
Length of boundary elements d	6.25 mm
Small distance h	0.1221 mm
Sampling points interval	0.1 m
Sound speed	340 m/s
Spatial Nyquist frequency	1700 Hz
Sound source frequency	1000, 1500, 2000, 4000 Hz

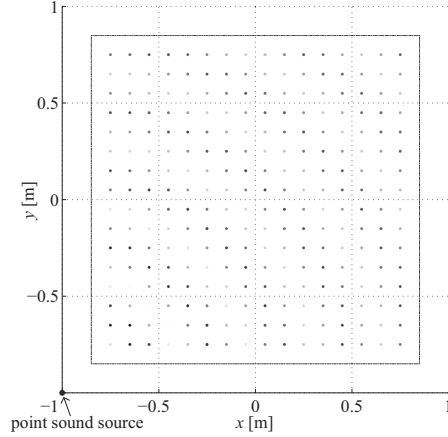


Fig. 4. Setting of the sampling points and the boundary for the numerical simulation in Section 4.1.

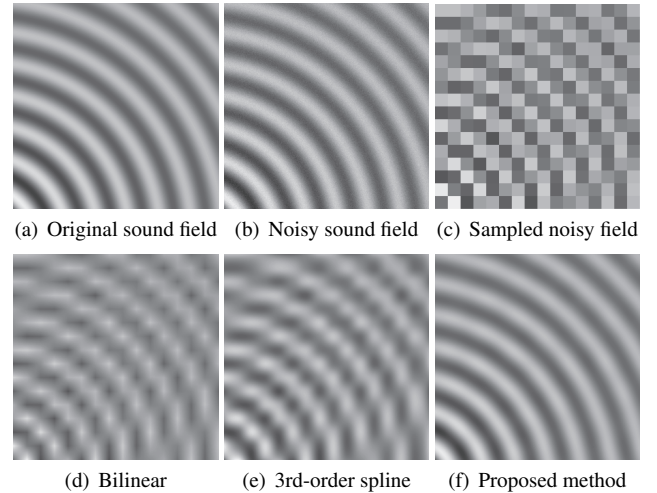


Fig. 5. A visual example of the simulation for 1500 Hz in Section 4.1. Normalized sound pressure is depicted as white for 1 and black for -1 : (a) original sound field, (b) noisy sound field composed by adding (a) and Gaussian noise whose SNR was 20 dB, (c) sampled noisy sound field, (d) interpolation results by bilinear interpolation, (e) third-order spline interpolation and (f) the proposed method.

From the results, it can be confirmed that the proposed method clearly outperforms bilinear and third-order spline interpolation for every frequencies. $\text{SNR}_{\text{result}}$ of the proposed method depicted in Fig. 5(f) is 25.22 dB, which is an example showing that it is difficult to find a difference between the original and the interpolated sound field visually when its $\text{SNR}_{\text{result}}$ is higher than around 20 or 25 dB.

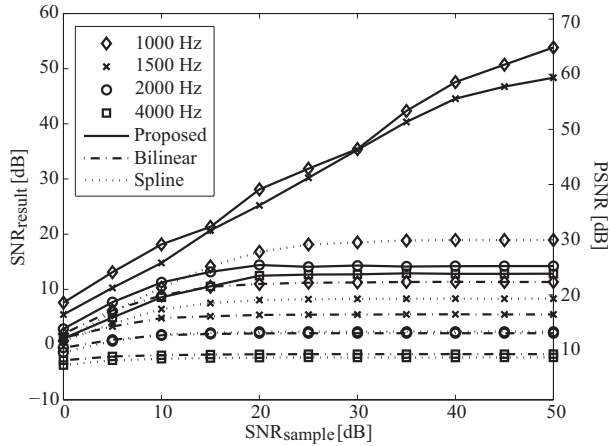


Fig. 6. SNR_{result} and PSNR of interpolated sound fields by bilinear interpolation, third-order spline interpolation and the proposed method in Section 4.1.

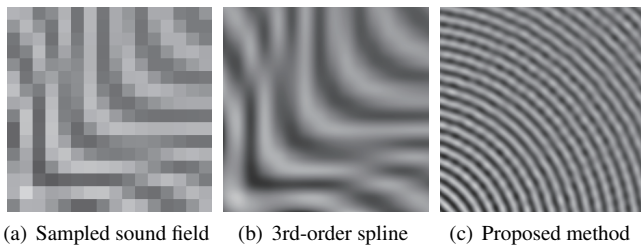


Fig. 7. A visual example of the simulation for a sound field produced by a 4000 Hz point sound source located as in Fig. 4.

Table 2. Measurement condition.

Place for measurement	Reverberation room @Waseda Univ. Honjo campus
Loud speaker	YAMAHA MSP5 STUDIO
Scanning LDV	Polytec PSV-300
Measured points	25×25 (= 625) points
Sound source frequency	2000 Hz

For the sound field whose frequency is under the spatial Nyquist frequency, 1700 Hz in this case, it can be reconstructed accurately especially when the data are less contaminated. On the contrary, the sound field exceeding the Nyquist frequency cannot be reconstructed from the data sampled by equal interval sampling points. However, the proposed method can still correctly sketch the image of the sound field exceeding the Nyquist frequency as shown in Fig. 7.

4.2. Application to real data

The proposed method is applied to real data recorded by a LDV. The measurement condition and setup are illustrated in Table 2 and Fig. 8. A Laser beam was emitted from the LDV to a light reflector stuck on the thick rigid cement wall of the huge (12 m × 20 m × 6.5 m) reverberation room. A stationary sound field driven by a 2000 Hz sinusoidal wave was recorded by 25 × 25 = 625 sampling points.

The results are shown in Fig. 9. The measured data were thinned out one-by-one and two-by-two in order to confirm properness of the proposed method. As the data reduced, third-order spline interpolation lost reproducibility of the measured sound field. In addition, spline interpolation was easily affected by measurement noise. In contrast, the proposed method can reproduce highly similar interpo-

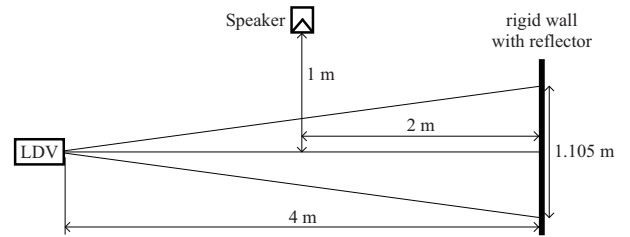


Fig. 8. Setup of the experiment described in Section 4.2.

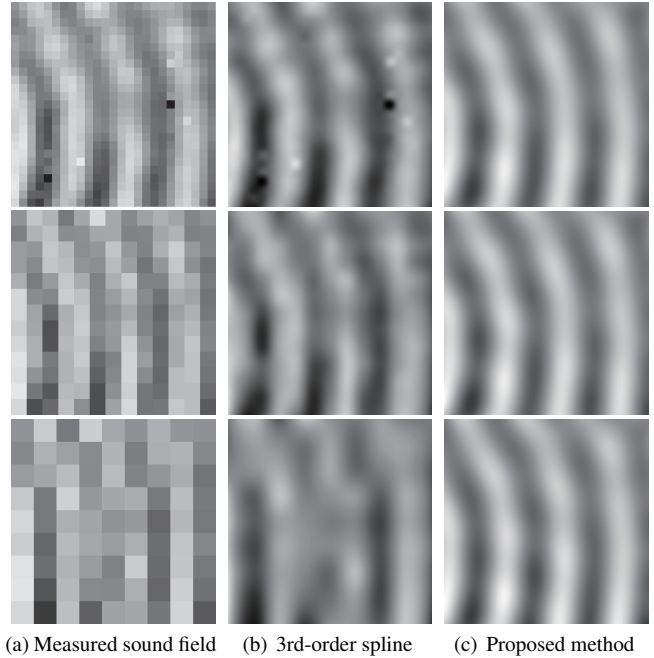


Fig. 9. An actual sound field measured by the LDV in Section 4.2. The top left figure illustrates the full 25 × 25 measured data and its interpolation results are illustrated on the top row. The middle row represents the results for reduced 13 × 13 data created by skipping the full data one-by-one. The lowest row is the results for reduced 9 × 9 data created by skipping the full data two-by-two.

lated fields from the reduced data without influence of noise. This result shows that almost 90 % of the measuring points can be reduced to achieve a similar result in this situation.

5. CONCLUSIONS

In this paper, a novel interpolation method for an optically measured sound field was proposed. The proposed method effectively utilizes the fact that the measured data represent a sound field by formulating the least squares method of the Kirchhoff-Helmholtz integral equation with a penalty term of the Helmholtz equation, while the conventional polynomial interpolation does not consider the behavior of data. The numerical simulation confirmed that the proposed method clearly outperformed the conventional methods especially when the noise level of the data was low. The effectiveness of the proposed method was also confirmed by the real data.

Future work will include improvement on the formulation of the optimization problem to handle the constraint of the Helmholtz equation more effectively. Furthermore, three-dimensional reconstruction of a sound field from optically projected two-dimensional data will be considered.

6. REFERENCES

- [1] M.J. Hargather, G.S. Settles, and M.J. Madalis, "Schlieren imaging of loud sounds and weak shock waves in air near the limit of visibility," *Shock Waves*, vol. 20, no. 1, pp. 9–17, Feb. 2010.
- [2] B.H. Pandya, G.S. Settles, and J.D. Miller, "Schlieren imaging of shock waves from a trumpet," *J. Acoust. Soc. Am.*, vol. 114, no. 6, pp. 3363–3367, Dec. 2003.
- [3] Y. Sonoda and M. Akazaki, "Measurement of low-frequency ultrasonic waves by fraunhofer diffraction," *Jpn. J. Appl. Phys.*, vol. 33, no. 5B, pp. 3110–3114, May 1994.
- [4] Y. Sonoda and Y. Nakazono, "Development of optophone with no diaphragm and application to sound measurement in jet flow," *Advances in Acoustics and Vibration*, vol. 2012, no. 909437, pp. 1–17, 2012.
- [5] Y. Oikawa, M. Goto, Y. Ikeda, T. Takizawa, and Y. Yamasaki, "Sound field measurements based on reconstruction from laser projections," in *Int. Conf. Acoust., Speech Signal Process. (ICASSP)*. IEEE, Mar. 2005, vol. IV, pp. 661–664.
- [6] Y. Ikeda, M. Goto, N. Okamoto, T. Takizawa, Y. Oikawa, and Y. Yamasaki, "A measurement of reproducible sound field with laser computed tomography (in japanese)," *J. Acoust. Soc. Jpn.*, vol. 62, no. 7, pp. 491–499, Jul. 2006.
- [7] T. Sakoda and Y. Sonoda, "Visualization of sound field with uniform phase distribution using laser beam microphone coupled with computerized tomography method," *Acoust. Sci. & Tech.*, vol. 29, no. 4, pp. 295–299, Jul. 2008.
- [8] Y. Ikeda, N. Okamoto, M. Goto, T. Konishi, Y. Oikawa, and Y. Yamasaki, "Error analysis for the measurement of sound pressure distribution by laser tomography (in japanese)," *J. Acoust. Soc. Jpn.*, vol. 64, no. 1, pp. 3–7, Jan. 2008.
- [9] A. Torras-Rosell, S. Barrera-Figueroa, and F. Jacobsen, "Sound field reconstruction using acousto-optic tomography," *J. Acoust. Soc. Am.*, vol. 131, no. 5, pp. 3786–3793, May 2012.
- [10] A. Torras-Rosell, S. Barrera-Figueroa, and F. Jacobsen, "An acousto-optic beamformer," *J. Acoust. Soc. Am.*, vol. 132, no. 1, pp. 144–149, July 2012.
- [11] Y. Ikeda, N. Okamoto, T. Konishi, Y. Oikawa, Y. Tokita, and Y. Yamasaki, "Observation of traveling wave with laser tomography (in japanese)," *J. Acoust. Soc. Jpn.*, vol. 64, no. 3, pp. 142–149, Mar. 2008.